# Molecular and cellular mechanisms by which cardiac sympathetic denervation prevents heart failure and sudden cardiac arrest

Deeptankar DeMazumder, MD, PhD [2,4]*, Pooja Joshi, PhD [1,2], Brian O'Rourke, PhD [3], Shanea Estes, BA [1,2], Swati Dey, PhD [1]*

1. Division of Clinical Pharmacology, Department of Medicine, Vanderbilt University Medical Center, Nashville, Tennessee.
2. Section of Cardiac Electrophysiology, Division of Cardiovascular Health and Disease, Department of Internal Medicine, University of Cincinnati College of Medicine, Cincinnati, Ohio.
3. Division of Cardiology, Department of Medicine, Johns Hopkins University School of Medicine, Baltimore, Maryland.
4. Section of Cardiac Electrophysiology, Division of Cardiology, Department of Internal Medicine, Richard L. Roudebush Veterans Affairs Medical Center, Indiana Institute for Medical Research, Indianapolis, Indiana.

* **Co-Corresponding Authors:**
Swati Dey, PhD
Division of Clinical Pharmacology, Department of Medicine
Vanderbilt University Medical Center
2215B Garland Avenue
Nashville, Tennessee 37203
Swati.Dey@vumc.org

Deeptankar DeMazumder, MD, PhD
Section of Cardiac Electrophysiology
Division of Cardiology, Department of Internal Medicine
Richard L. Roudebush Veterans Affairs Medical Center
Indiana Institute for Medical Research
1481 West 10th Street, Room# D-3040 (mail code 151)
Indianapolis, Indiana 46202
Deeptankar.DeMazumder@va.gov

**Short Title:** CSD mitigates mROS, diastolic $Ca^{2+}$, SCA and HF

**Funding Support:** This study was supported by grant awards from the National Institutes of Health (NIH) Common Fund Director's New Innovator Award DP2 HL157941, NIH National Heart, Lung, and Blood Institute (NHLBI) 4R00HK130662, American Heart Association (AHA) Transformational Project Award 19TPA34850151 and Department of Defense (DOD) W81XWH-201-0701 #PR191442.

**Acknowledgements:** SD and DD jointly conceived and designed this study and wrote the manuscript; PJ and SE performed blinded analyses and interpreted results; All authors reviewed/revised the manuscript.

**Disclosures:** None of the authors have any disclosures or conflict of interest.

**Current Words:** Abstract=328/350; Text=3,360/5,000; References=50; Figs=6.

## ABSTRACT

***Rationale:*** Sudden cardiac arrest (***SCA***) and heart failure (***HF***) are leading causes of death. The underlying mechanisms are incompletely understood, limiting the design of effective therapies. Whereas most autonomic modulation therapies have failed to show benefit in HF patients, a growing body of clinical evidence over the past 50 years suggests cardiac sympathetic denervation (***CSD***) confers cardioprotection. However, the underlying molecular and cellular mechanisms remain unexplored.

***Objective:*** Based on the hypothesis that mitochondrial reactive oxygen species (***mROS***) drive the pathogenesis of HF and SCA, we investigate whether CSD prevents SCA and HF by improving mitochondrial antioxidant capacity and redox balance, to correct impaired $Ca^{2+}$ handling and repolarization reserve.

***Methods and Results:*** We interrogated CSD-specific responses in pressure-overload HF models with spontaneous SCA using *in vivo* echocardiographic, electrocardiographic, biochemical (e.g., mitochondrial antioxidant and NADPH producing enzymes) and *in vitro* studies, including dynamic measures of ratiometric mROS, $Ca^{2+}$ and sarcomere length in left ventricular myocytes. Hemodynamic compromise in HF increased mROS levels, which impaired β-adrenergic signaling and increased sarcoplasmic reticulum $Ca^{2+}$ leak, thereby reducing sarcoplasmic $Ca^{2+}$ load, increasing diastolic $Ca^{2+}$, impairing myofilament contraction and further increasing the sympathetic stress response. Importantly, diastolic $Ca^{2+}$ levels were more important than sarcoplasmic $Ca^{2+}$ for driving the beat-to-beat variability of $Ca^{2+}$ transients and triggering arrhythmogenic activity. Surgical CSD protected against HF progression by upregulating mROS antioxidant and NADPH producing enzymes that, in turn, mitigated diastolic $Ca^{2+}$ overload, triggered activity and dispersion of repolarization.

***Conclusions:*** Our findings support a fundamental role of sympathetic stress-induced downregulation of mROS scavenging enzymes and RyR-leak mediated diastolic $Ca^{2+}$ overload in the pathogenesis of HF and SCA that is abolished by CSD. This first report on the molecular and cellular mechanisms of CSD therapy supports the evaluation of its utility in a broader group of high risk patients. Our findings may be generalizable to other forms of cardiomyopathy and arrhythmias. Further studies on targets engaged by CSD may advance the design of new, more effective therapies for cardiomyopathy and arrhythmias.



## BRIEF SUMMARY

Clinical evidence suggests cardiac sympathetic denervation (***CSD***) confers cardioprotective effects, such as preventing heart failure (***HF***) and sudden cardiac arrest (***SCA***). The underlying molecular and cellular mechanisms are unknown, limiting optimal clinical application. We hypothesized that CSD prevents SCA and HF by improving mitochondrial antioxidant capacity, autonomic and redox balance, $Ca^{2+}$ handling and repolarization reserve. In a guinea pig model that uniquely mimics human HF with spontaneous SCA, we interrogated CSD-specific responses using echocardiographic, electrocardiographic, biochemical, and dynamic ratiometric measures of mitochondrial reactive oxygen species (***mROS***), $Ca^{2+}$ and sarcomere length in cardiomyocytes. Surgical CSD rescued cardioprotection by upregulating mROS antioxidant and NADPH producing enzymes, which mitigated mROS-induced diastolic $Ca^{2+}$ overload, triggered activity, repolarization lability, HF and SCA. Our findings show a critical mechanistic role of diastolic $Ca^{2+}$ that may be broadly applicable to other cardiomyopathies and arrhythmias, and provide the first molecular and cellular mechanistic basis to support CSD therapy more broadly in high-risk patients.



## KEYWORDS

Autonomic nervous system, stellate ganglionectomy, sympathetic denervation, autonomic modulation, diastolic $Ca^{2+}$, ventricular tachycardia, ventricular fibrillation, sudden cardiac death

The sympathetic "fight-or-flight" stress response triggers the release of hormones that produce well-orchestrated changes throughout the body. Acute increases in sympathetic stress improve cardiovascular function. However, persistent sympathetic hyperactivity becomes maladaptive, increasing the risk of heart failure (***HF***) and sudden cardiac arrest (***SCA***)[1]. Despite optimal medical therapy, half of all HF patients die within 5 years of diagnosis and SCA accounts for about half of these deaths. The need for the design of new, more effective therapies for these two leading causes of death in the industrialized world remains a clinical, research and public health priority.

Most HF therapies aimed at curbing sympathetic hyperactivity have had limited success. Drugs for blocking β-adrenergic receptors and the renin-angiotensin-aldosterone system delay mortality, but do not reverse HF progression. Implantable device-based autonomic modulation, such as vagal nerve and spinal cord stimulation, initially showed promising results in preclinical studies but ultimately, failed to improve left ventricular (***LV***) function in clinical trials of HF patients. In the context of SCA, current therapies are even more limited. β-adrenergic receptor blockers do not prevent SCA. Antiarrhythmic drugs are often proarrhythmic and actually increase long-term mortality. Progress in designing new therapies has been limited by poor mechanistic insight into the molecular and cellular effects of modulating sympathetic hyperactivity on the heart.

A large body of evidence over the past century[2-4] suggests cardiac sympathetic denervation (***CSD***) protects against HF[5-13] and SCA[13-17]. Despite these extensive studies, the underlying molecular and cellular mechanisms by which CSD confers cardioprotective effects have remained unexplored. As such, current application of CSD is limited to a small subset of high risk patients[4, 8-12, 15, 18-20]. An improved understanding of the molecular and cellular mechanisms can be used to improve its efficacy, extend its application to a broader patient population, and identify key molecular targets engaged by CSD to better understand the underlying pathophysiology and design new, more effective therapies.

Our recent work[21] showed that mitochondrial reactive oxygen species (***mROS***) drive the pathogenesis of HF and SCA, involving derangements of autonomic and redox balance, $Ca^{2+}$ handling, and electrical stability. The precise functional consequences are unclear. Whether CSD engages this signaling pathway to confer salutary effects is unknown. We hypothesized that CSD prevents SCA and HF by improving mitochondrial antioxidant capacity, autonomic and redox balance, $Ca^{2+}$ handling, and cardiac repolarization reserve. This first report of the molecular, cellular and systemic mechanisms of CSD's cardioprotective effects illustrates the critical role of mROS-induced diastolic $Ca^{2+}$ overload in the pathogenesis as well as effective therapy of both HF and SCA.

**<u>Animal models of HF and SCA</u>:** The foremost limitation for mechanistic studies of HF and SCA has been the lack of a suitable experimental model that mimics its human counterpart[22]. Genetic models have contributed important mechanistic insight, but most SCA victims do not have well-defined genetic abnormalities. Based on current clinical guidelines, HF patients with poor LV systolic function are eligible for primary prevention ICD implantation. However, most SCA victims do not have HF and remain asymptomatic until catastrophic clinical presentation. Moreover, the primary etiology of human HF is non-ischemic, e.g., involving antecedent uncontrolled hypertension[23]. Non-ischemic VT is also more challenging to treat clinically, and the underlying mechanisms of non-ischemic HF and VT are poorly understood. To address this unmet need, we established a guinea pig pressure-overload model that recapitulates keys features of human HF and SCA[21]. Unique to this model is a high incidence of spontaneous VT, leading to SCA in freely ambulating animals. The VT episodes start occurring early during HF development. Our recent transcriptomic, proteomic, metabolomic, and functional studies demonstrated that this model recapitulates key features of human HF, including derangements of autonomic,

electrophysiological, hormonal, $Ca^{2+}$ handling, energetic, redox, metabolic, extracellular matrix, and inflammatory components as an integrative maladaptive response to cardiac insult. We further showed that high mROS levels cause chronic proteome remodeling, leading to impaired contractility, and post-translational modifications, increasing the risk of VT and SCA. Notably, the VT burden is highest after, but not during, mild transient β-adrenergic stress, as also noted in humans. Thus, this model represents an ideal platform to investigate the salutary effects of CSD on HF and SCA.

**Interventions:** Using this model, we performed video-assisted thoracoscopic surgery to mimic the clinical CSD procedure for bilateral excision of the inferior half of the stellate ganglion (**Fig. 1A**), a discrete bundle of nerve cells near C7-T1 that provides the major sympathetic input to the heart. Surgical accuracy was confirmed by prototypical perioperative functional responses (**Fig. 1B**), i.e., graded change in heart rate after unilateral and bilateral sympathectomy (**Fig. 1-B**), and postoperative immunostaining for tyrosine hydroxylase (***TH***), neurofilament (***NF***) and 4',6-diamidino-2-phenylindole (***DAPI***), which showed that the excised tissue section encompassed sympathetic neurons (**Fig. 1-C**).

We randomized the animals to 5 groups: (**1**) normal controls with sham CSD (***normal+shamCSD***); (**2**) normal controls with CSD (***normal+CSD***), (**3**) HF with sham CSD surgery (***HF+shamCSD***), (**4**) HF with CSD (***HF+CSD***) to abolish sympathetic hyperactivity, or (**5**) HF with continuous mROS scavenging *in vivo* with MitoTEMPO (***HF+mROS-scavenging***) for reducing global cellular oxidative stress[21, 24]. The primary endpoint was VT-free survival at 4 weeks. Cardiac mROS responses were assessed in LV myocytes from HF+shamCSD and HF+CSD models with or without acute exposure to isoproterenol, for increasing endogenous ROS, or to graded amounts of exogenous ROS ($H_2O_2$) to measure antioxidant activity.

Because an *in vivo* model of HF+CSD with controlled increases in cardiac mROS does not currently exist, we interrogated LV myocytes from HF+shamCSD and HF+CSD models *in vitro* using isoproterenol (for generating endogenous ROS) or $H_2O_2$ (for graded amounts of exogenous ROS).

**CSD improves LV function:** Cardiac contractile function was measured in conscious animals using serial echocardiography (**Supplementary Fig. 1**). The HF+shamCSD group developed LV hypertrophy over the first 2 weeks that then progressed to dilated cardiomyopathy over the next 2 weeks (**Fig. 1D-F**). HF induced changes typical of dilated cardiomyopathy, including increases in LV systolic and diastolic volumes, and decreased stroke volume, ejection fraction and fractional shortening. CSD improved LV structure and systolic function, and prevented dilated cardiomyopathy, consistent with reports in HF patients[5-13].

**CSD mitigates SCA:** Adjudication of continuous *in vivo* electrocardiography (***ECG***), obtained via wireless implanted telemetry devices in freely ambulating animals, revealed spontaneous episodes of premature ventricular contractions (***PVCs***) and VT in the HF+shamCSD group (**Fig. 1G**), occurring as early as the first week (i.e., before any apparent signs of LV dysfunction) and leading to SCA in >70% of animals by the fourth week (**Fig. 1H**). As discussed above, these findings are similar to humans in that the majority of victims do not have HF at the time of SCA. As also noted in patients[13, 15-17], CSD mitigated VT and SCA. These lifesaving effects were recapitulated by *in vivo* mROS scavenging (**Fig. 1E-H**), suggesting mROS is involved in the mechanistic pathway for CSD effects.

**CSD improves cardiac autonomic balance:** In normal animals, CSD had no apparent effect on ECG-derived heart rate variability (***HRV***) and sympathovagal balance (**Supplementary Fig. 2**), suggesting a large margin of safety for cardiac sympathetic input along with dominant parasympathetic control of resting hearts. By contrast, the hemodynamic compromise in HF+shamCSD increased heart rate and sympathetic tone, reduced HRV and total power, and blunted the chronotropic response to brief (1-hour) β-adrenergic stress caused by administration of low-dose isoproterenol via an implanted automated wireless pump.

Notably, VT and SCA episodes occurred more frequently over the several hours following, but not during, β-adrenergic stress. These findings are also in agreement with those reported in human HF[11, 19, 25].

Despite pressure-overload induced hemodynamic compromise, CSD improved the heart rate (**Figs. 2A-G**), HRV (**Figs. 2H-I**), sympathovagal balance (LF/HF ratio; **Figs. 2J-K**), total power (**Figs. 2L-M**), and chronotropic response to β-adrenergic stress (**Fig. 2C,G**). Again, *in vivo* mROS scavenging yielded similar results to CSD (**Fig. 2**), raising the possibility that CSD reduces mROS levels and improves β-adrenergic receptor-mediated signaling by enhancing the mitochondrial antioxidant capacity of LV myocytes. Thus, we performed molecular and cellular studies to address this question.

**CSD improves redox balance by increasing mitochondrial antioxidant capacity:** We tested this hypothesis by quantifying ROS ($H_2O_2$) dynamics in intracellular compartments of LV myocytes at the highest spatiotemporal resolutions[21, 24]. Briefly, we performed *in vivo* viral transduction of a genetically-encoded sensor, mitoORP, which is a ratiometric $H_2O_2$ sensor with dual-excitation wavelengths of 405 and 488 nm and emission at 520 nm. Each experiment was calibrated for the minimum and maximum wavelengths (405/488 nm ratio). Fractional oxidation of the sensor ($F_{ox}$) was calculated to facilitate quantitative comparisons of basal and stimulated mROS levels across experimental groups.

Compared to normal hearts, the LV myocytes from pressure overloaded hearts had high mROS levels (HF+shamCSD, $F_{ox}$=0.59±0.02), which were mitigated by CSD (HF+CSD, $F_{ox}$=0.38±0.03; $p<0.01$) (**Fig. 3A-C**). To determine whether CSD reduced mROS by increasing mitochondrial antioxidant capacity, we increased the generation of endogenous mROS by exposing the myocytes to isoproterenol (1 μM) with electrical field stimulation. Compared to HF+shamCSD ($F_{ox}$: 0.44±0.03), mROS levels remained much lower in HF+CSD myocytes ($F_{ox}$: 0.71±0.03; $p<0.001$) (**Fig. 3D**). Further, we confirmed these findings by treating the myocytes with exogenous ROS (tert-butyl hydroperoxide, 1 mM). Again, the mROS levels remained significantly lower in HF+CSD ($F_{ox}$: 0.48 ± 0.02) compared to HF+shamCSD myocytes ($F_{ox}$: 0.84 ± 0.03, $p<0.001$) (**Fig. 3E**).

To identify the molecular basis for the CSD-mediated preservation of mitochondrial antioxidant capacity, we quantified mRNA expression levels of mitochondrial antioxidant and NADPH producing enzymes (**Fig. 3F**). Whereas the expression of glutathione peroxidase (GPX4), peroxidase (PRX3), thioredoxin reductase (TXNRD2), malic enzyme 3 (ME3) and nicotinamide nucleotide transhydrogenase (NNT) were reduced in HF+shamCSD animals but not in HF+CSD animals.

These findings indicate that reduced mROS scavenging is a critical pathogenic component of HF and that CSD exerts its cardioprotective effects, at least in part, by enhancing mitochondrial antioxidant capacity and reducing mROS levels in LV myocytes. We previously showed that high mROS levels control global cellular oxidative stress, leading to wide spread damage, including derangements in $Ca^{2+}$ handling and β-adrenergic receptor-mediated signaling[21, 24]. Further, ROS oxidizes thiol groups of cysteine residues on ryanodine receptors (***RyRs***)[26-28], augmenting spontaneous $Ca^{2+}$ leak from the sarcoplasmic reticulum (***SR***) during diastole[28] that in turn, increases diastolic $Ca^{2+}$ levels[29]. High diastolic $Ca^{2+}$ activates a transient inward current involving primarily the Na-Ca exchanger, resulting in delayed afterdepolarizations (***DADs***)[30], which can induce other triggered activity (i.e., early afterdepolarizations) and repolarization lability, leading to VT and SCA. Indeed, the arrhythmogenic effects of cardiac glycosides involve mROS generation and RyR oxidation[31]. Although prior studies have reported acute increases in ROS generation with isoproterenol, whether ROS induced by sympathetic hyperactivity in HF, and its downstream effects on SR $Ca^{2+}$ handling, can be reversed by CSD has not been tested.

**CSD improves SR $Ca^{2+}$ load, β-adrenergic responsiveness and sarcomere shortening:** The HF+shamCSD myocytes exhibited $Ca^{2+}$ transients with slower upstrokes (reflecting reduced SR $Ca^{2+}$ load),

blunted peaks, prolonged decays (**Fig. 4A-E**), and blunted responses to maximal β-adrenergic receptor activation (**Fig. 4F-I**), along with similar impairments in sarcomere shortening (**Fig. 4J-R**). CSD improved $Ca^{2+}$ transient upstroke, peaks and decays. The consequent faster and larger $Ca^{2+}$ transients, in the absence and presence of β-adrenergic stimulation, improved myofilament contractions, as evidenced by increased sarcomere shortening of LV myocytes (**Fig. 4J-R**), accounting for the increase in global LV systolic function (**Fig. 1E-F**).

**CSD reduces triggered activity and dispersion of repolarization by reducing ROS-mediated SR $Ca^{2+}$ leak-induced diastolic $Ca^{2+}$ overload:** To determine the mechanistic link between ROS, SR $Ca^{2+}$ leak, diastolic $Ca^{2+}$, and arrhythmic risk, we induced endogenous ROS generation or added exogenous ROS to LV myocytes and evaluated the incidence of disturbances in $Ca^{2+}$ transients and sarcomere shortening, such as delayed after-transients and after-contractions (**Fig. 5A**). Further, we quantified beat-to-beat dispersion in $Ca^{2+}$ transient duration (***dCaTd***) by its coefficient of variation (CV), calculated as 5-transient bins of the mean divided by the standard deviation of the time from the $Ca^{2+}$ transient's peak to the time to return to 80% diastolic $Ca^{2+}$ level (**Fig. 5B**). These disturbances, occurring more often in HF+shamCSD compared to HF+CSD myocytes (25% vs. 5%; $p<0.001$), were reversibly suppressed by *in vitro* ROS scavenging (**Fig. 5B-C**). Whereas increasing ROS increased diastolic $Ca^{2+}$, scavenging ROS lowered pacing-induced diastolic $Ca^{2+}$ (**Fig. 5B-C**), suggesting a direct mechanistic link. Mitochondrial ROS appeared to be the upstream effector of RyR-mediated leak and the diastolic Ca increase because when caffeine increased the RyR leak **(Fig. 5-B)** mROS scavenging was no longer effective. Further, dantrolene, which stabilizes RyRs to prevent SR $Ca^{2+}$ leak during diastole, eliminated these disturbances despite high mROS levels, indicating that the diastolic SR $Ca^{2+}$ leak via RyRs was the mediator of the triggered activity.

In HF+shamCSD myocytes, the high mROS levels strongly correlated with pacing-induced diastolic $Ca^{2+}$ levels (**Fig. 5D**), which strongly correlated with dCaTd (**Fig. 5E**), in association with a higher incidence of triggered activity when pacing-induced diastolic $Ca^{2+}$ and dCaTd were high. However, dCaTd and triggered activity correlated poorly with peak systolic $Ca^{2+}$ levels (**Fig. 5F**), suggesting diastolic $Ca^{2+}$ drives dCaTd and triggered activity. Importantly, treatment with CSD abolished these associations and markedly lowered pacing-induced diastolic $Ca^{2+}$ and dCaTd (**Fig. 5G-H**), along with lower mROS levels (**Fig. 3A-C**).

Consistent with the *in vitro* findings, HF+shamCSD animals exhibited prolonged repolarization and increased dispersion of repolarization, as indexed by beat-to-beat changes in the ECG's QT interval (**Fig. 5I**), in association with a higher incidence of VT (**Fig. 1G-H**). Notably, CSD did not shorten repolarization (**Fig. 5J**) but reduced its dispersion (**Fig. 5K**), and reduced 24-hour PVC burden (**Fig. 5L**). In a prior multicenter prospective study of HF patients, we demonstrated that increased dispersion of repolarization strongly predicts SCA, independent of other clinical parameters including the QT interval[32].

Together, our results strongly support the hypothesis that high mROS levels during sympathetic stress increase diastolic $Ca^{2+}$ via RyR-mediated SR $Ca^{2+}$ leak that, in turn, causes electrical instability, triggered activity, and dispersion of $Ca^{2+}$ transients and repolarization, resulting in VT and SCA; CSD rescues cardioprotection by reducing the mROS-induced SR $Ca^{2+}$ leak and lowering diastolic $Ca^{2+}$ levels.

## DISCUSSION

Despite growing clinical use[2-20], the mechanistic link between surgical CSD therapy for modulating sympathetic hyperactivity, HF and SCA has been unexplored. As such, current use of CSD therapy is limited to a small subset of high risk patients (i.e., those with long QT syndrome, catecholaminergic polymorphic VT, arrhythmogenic right ventricular cardiomyopathy, and refractory VT requiring recurring defibrillator shocks despite optimal therapy with β-adrenergic receptor blockers and catheter ablation[4, 8-12, 15, 18-20]). The

present study provides the first molecular, cellular and systemic mechanistic basis to support the clinical efficacy of CSD for treating HF[5-13] and SCA[2, 3, 13-17], i.e., by upregulating mitochondrial antioxidant and NADPH producing enzymes to improve mROS scavenging, reducing mROS levels to prevent SR $Ca^{2+}$ leak through RyR, in turn improving sarcoplasmic $Ca^{2+}$ load and β-adrenergic responsiveness. Together, these CSD effects improve LV systolic function, and more importantly, lower diastolic $Ca^{2+}$, which drives the beat-to-beat variability in $Ca^{2+}$ transient duration and triggered activity. The instability of diastolic $Ca^{2+}$ handling could also further exacerbate mROS in a vicious cycle[33-35]. The prevention of mROS-induced diastolic $Ca^{2+}$ leak by CSD reduces heterogeneity of $Ca^{2+}$ transient duration, trigged activity, dispersion of repolarization and SCA (**Fig. 6**). These findings have broad relevance to the potential utility of using CSD therapy in high-risk patient populations, incluidng non-ischemic HF, high SCA risk patients not eligible for primary ICD implantation based on current clinical guidelines, early stages of LV dysfunction and HF. These findings also highlight the critical role of sympathetic stress-induced high mROS-mediated diastolic $Ca^{2+}$ overload in the pathogenesis of HF and SCA.

During acute stress, sympathetic nerves release norepinephrine to active cardiac β-adrenergic receptor-adenylate cyclase–cAMP–protein kinase A signaling, which phosphorylates excitation-contraction coupling proteins such as SERCA, phospholamban, LTCC and RyRs. The consequent increase in LTCC $Ca^{2+}$ flux and SR $Ca^{2+}$ load, along with synchronization of SR $Ca^{2+}$ release[36] during systole, elicits positive inotropy to meet physiological demands. By contrast, during chronic sympathetic stress, persistent activation of β-adrenergic receptors becomes maladaptive[21,37], increasing energy demand and workload, which in turn, generate mROS, a main source of oxidative stress in the heart[17,24]. The consequent increases in ATP and NADPH consumption weaken mitochondrial antioxidant defense. Importantly, we showed previously[21], and in the present study, that mROS scavenging capacity is further reduced by downregulation of mitochondrial antioxidant enzymes. Beyond a certain threshold, as the rate of mROS generation exceeds the rate of mROS scavenging, the excess mROS released from the mitochondrion propagate to and induce ROS generation in other mitochondria and intracellular compartments. This regenerative positive-feedback cycle (ROS-induced ROS release[38]) increases global cellular ROS and oxidizes multiple ion channels/transporters.

Notably, the RyRs, in close proximity to, and tightly coupled with, the mitochondrial network, are readily modified by ROS[26-28], via direct oxidation of thiol groups of cysteine residues[26, 28] as well as ROS-mediated $Ca^{2+}$-independent activation of CaMKII[39], increasing SR $Ca^{2+}$ leak[40] to promote VT[41]. A key finding in the present study is that mROS-induced RyR-mediated increases in diastolic $Ca^{2+}$ drive arrhythmic risk via dispersion of $Ca^{2+}$ transient decay and membrane repolarization, DADs[30, 37], $Ca^{2+}$ waves and triggered activity. The spatiotemporal dispersion of repolarization between regions with the highest $Ca^{2+}$ load (generating spontaneous SR $Ca^{2+}$ release) and regions with lower $Ca^{2+}$ load may also promote VT. The depletion of SR $Ca^{2+}$ load blunts the rapid rise in $Ca^{2+}$ in the diadic space, impairing mitochondrial $Ca^{2+}$ signaling and increasing mROS. Surgical CSD mitigates this vicious ROS-mediated cycle of widespread damage and protects against HF/SCA by: (1) increasing the rate of mROS scavenging by upregulating mitochondrial antioxidant and NADPH producing enzymes; (2) reducing mROS-induced SR $Ca^{2+}$ leak to improve SR $Ca^{2+}$ load, β-adrenergic signaling and chronotropic competency, thereby improving LV contractility; and (3) mitigating diastolic $Ca^{2+}$ overload, dispersion of $Ca^{2+}$ transients and repolarization, and SCA risk.

Scavenging mROS *in vivo*, a potential therapeutic strategy[42, 43], conferred salutary effects similar to those of CSD. It is noteworthy that ROS are not only involved in pathological processes but also participate in normal physiological signaling[44]. Calcium handling in healthy cardiomyocytes is especially sensitive to ROS levels, such as RyR activation and SERCA inhibition[27] and modulation of LTCC function[45]. Even

small increases in mROS have important physiological roles such as increasing mitochondrial biogenesis, regulating mitochondrial respiration, lipolysis and differentiation, and inducing proton leak without damaging the mitochondrial membrane[46, 47]. As such, excessive ROS scavenging could disturb signaling processes that are beneficial for cell function. For example, excessive overexpression of mitochondrially-targeted catalase has been linked to impaired mitophagy[48]. The present findings indicate that CSD lowers oxidative stress without limiting the necessary ROS-dependent physiological processes. Modulating sympathetic/parasympathetic tone via implantable nerve stimulators or CSD could, therefore, could be a viable and safe therapeutic intervention for modulating cardiac oxidative stress and its downstream effects on cardiac transcriptome/proteome remodeling, contractile function, and life-threatening arrhythmias.

**Limitations:** A potential limitation of the present study is that surgical CSD was performed at the onset of pressure-overloaded HF. High risk patients are typically brought to clinical attention at more advanced HF stages (e.g., dilated cardiomyopathy). However, the risk of SCA is especially high during early stages of remodeling, i.e., before LV function has declined. Indeed, the majority of SCA victims have little or no impairment in LV function. These patients are also the most challenging to study because they are routinely misclassified as being lower risk by conventional clinical criteria[49, 50]. Thus, our findings have important clinical implications for this larger, yet underexplored high-risk group. Future studies will determine whether CSD activates the same cardioprotective pathways after onset of advanced HF.

**Conclusions:** Chronic sympathetic stress drives the pathogenesis of HF and SCA by downregulating mitochondrial antioxidant enzymes. The consequent increase in mROS levels induces RyR $Ca^{2+}$ leak, reducing SR $Ca^{2+}$ load and systolic function and further increasing the stress response, but also increasing diastolic $Ca^{2+}$, which causes dispersion of $Ca^{2+}$ transients, DADs and triggered activity in LV myocytes, and globally, dispersion of repolarization and VT. The CSD-mediated engagement of these mechanistic targets provides strong mechanistic basis to support its clinical efficacy for preventing HF and SCA and extending its application to other high-risk populations. New pharmacological or pacing therapies may be designed for reversibly modulating sympathetic activity, mROS and diastolic $Ca^{2+}$, opening new avenues for HF and SCA therapy with remarkable implications for human health.

## METHODS

**Animal model:** Hartley guinea pigs (~300 grams) of either sex were used in accordance with IACUC-approved protocols at the University of Cincinnati and Johns Hopkins University. Briefly, anesthesia was induced and maintained with isoflurane. The pressure-overload HF model with ascending aortic constriction was created as previously described[21]. The animals were randomized to Sham vs. CSD procedures. CSD was performed in the HF+CSD group at the time of ascending aortic constriction surgery using video-assisted thoracoscopic surgery, by ablating and excising the inferior half of the stellate ganglion via a minimal thoracotomy without any damage to the ribs or surrounding structures. A Gemini Electrocautery system with tip temperatures up to 2,200°F was used to ablate and excise the lower half of the stellate ganglion. The procedure was then repeated on the contralateral side. The thoracic cavity was then closed. The CSD and Sham groups received similar incisions and could not be distinguished based on incision scars. Vital signs including ECG, $CO_2$ and pulse oximetry were monitored throughout the procedure. All personnel involved in post-surgical data collection and analysis were blinded to the CSD vs. Sham groups. Each animal was tracked via a unique computer-generated ID.

Adenoviruses for expression of the genetically-engineered cytosolic or mitochondrial $H_2O_2$ probes (cyto-ORP, mitoORP) were directly injected intramyocardially (100µl adenovirus suspension; 1-5 x $10^{10}$ virus particles) into the LV free wall with a 30G needle. *In vivo* probe expression was determined to be present for at least six weeks post injection.

An ECG transmitter (Data Sciences International ETA-F20 Biopotential Telemetry device) was implanted in the animal's abdominal cavity, and the leads were secured in a lead II arrangement. An iPRECIO programmable pump was implanted in the abdominal cavity for timed controlled delivery of pharmacological agents (e.g., isoproterenol, MitoTEMPO). When animals were breathing spontaneously after the procedure, bupronex (0.05mg/kg) was administrated via intramuscular injection for analgesia and animals were observed until full recovery.

**Vector construction:** The vectors for the compartment-specific roGFP-ORP1 ratiometric probes were constructed as previously described[21, 24]. Briefly, the yeast peroxidase (ORP1) sequence is fused downstream of the roGFP cassette by a 30 amino HF/SCA linker (GSSG)6. These probes were incorporated into adenoviral expression vectors for gene transfer in cells or tissues. The Mito-roGFP-ORP1 sequence was synthesized (Bioneer, Inc.) and cloned into a destination vector pAd/PL-DEST using two fragment Multisite Gateway Pro vector system technology (Invitrogen, Inc.). Mito-roGFP-ORP1 was cloned into a donor vector pDONR221P5-P2, resulting in an entry clone, pENTR(5-2)-Mito-roGFP-ORP1. Expression of roGFP-ORP1 was driven by an EFl-alpha promoter, cloned into another donor vector pDONR221P1-P5r, resulting in an entry clone pENTR(1-5r)-EF1alpha. In a second step, both entry clones and a destination vector pAd/PL-DEST were combined, resulting in the expression clone, pAd/PL-EF1alpha-Mito-roGFP-ORP1[3]. Replication-deficient adenovirus particles were produced from pAd/PL-EF1alpha-Mito-roGFP-ORP1 using the ViraPower Adenoviral Expression System (Invitrogen, Inc.).

**Echocardiography:** Echocardiography was performed (by operators blinded to the study groups) on conscious animals using a 20 MHz ultraband transducer interfaced with a Visual-Sonics Vevo 2100 imaging system. Two-dimensionally directed M-mode images were obtained from the long axis views. Comprehensive M-mode and two dimensional imaging was used to determine fractional shortening, wall thickness estimated wall mass, cardiac function, volumes, ejection fraction, cardiac output. Doppler flow imaging was used to assess systolic and diastolic function. Echocardiographic measurements were made on 3 consecutive cardiac cycles by the leading edge-to-leading edge method. LV end-diastolic and end-systolic dimensions, and LV end-diastolic posterior wall thickness, were measured from the M-mode images, and left fractional ventricular shortening was calculated with the software. Serial echo-Doppler studies to measure transaortic and transbanding pressure gradients and peak velocities were performed at baseline, 2 weeks and 4 weeks to verify model consistency.

**ECG**: Continuous ECG recordings were performed using wireless implanted devices (Data Sciences International, St. Paul MN). The data were exported and analyzed in a custom-developed MATLAB software (MathWorks, Inc., Natick, MA) to adjudicate the incidence of VT and SCA. Heart rate variability (HRV) analysis was performed in the time and frequency domains as previously described[32].

**Cardiomyocyte isolation, $Ca^{2+}$ transients and sarcomere shortening:** The LV myocytes were isolated from guinea pig hearts by enzymatic digestion, as described before[2]. Briefly, the freshly isolated LV myocytes were loaded with the ratiometric $Ca^{2+}$ indicator, Indo-1 AM (Life Technologies, Grand Island, NY) at room temperature. Myocyte sarcomere shortening and whole-cell $Ca^{2+}$ transients were assessed at 37°C with 1 Hz electrical stimulation using an inverted Olympus microscope equipped with fluorescence imaging (MyoCam, IonOptix) in the absence and presence of isoproterenol (β-adrenergic receptor agonist), or MitoTEMPO (mROS scavenger).

**Compartment specific, quantitative ROS measurements:** The mROS levels in LV myocytes were measured using genetically-encoded, ratiometric GFP probes, which detect physiological levels of local $H_2O_2$, as described previously[21, 24] . To test the compartment specific efficiency of antioxidant enzymes, LV myocytes from normal and failing hearts were challenged with 1mM tert-butyl hydroperoxide (exogenous

$H_2O_2$), a more stable form of peroxide that decreased experimental variability by minimizing spontaneous $H_2O_2$ decomposition. The myocytes were perfused with isoproterenol (1 μM) during electrical stimulation at 1 Hz and imaged every 10 sec, which minimized oxidative stress due to the imaging process itself. Images were collected at a 10 sec interval over 30 min. 405/488nm excitation ratio images were created and analyzed using ImageJ software (Rasband, W.S., ImageJ, U. S. National Institutes of Health, Bethesda, Maryland, U.S.A. http://imagej.nih.gov/ij/, 1997-2014) as 16-bit TIFF files. After normalization of the ratiometric signals to Rmax (1) and Rmin (0) to obtain the fractional oxidation ($F_{ox}$) of the sensor, the change in roGFP-ORP1 signal from baseline (ΔFox) was determined for the various oxidative challenges.

**Molecular studies:** We performed quantitative PCR (qPCR). The RNA was isolated from LV myocardium using Trizol (Invitrogen) and 1-Bromo-3-Chloropropane (Molecular Research Center Inc.), then reverse transcribed (High Capacity cDNA Reverse Transcription Kit, Applied Biosystems). Guinea Pig B2M gene was used as a housekeeping gene. Pre-designed primers targeted to guinea pig TH, ChAT, IDH2, ME3, NNT, Txnrd2, Prdx3, Gpx4 were ordered from Sigma.

**Statistical analysis:** A goodness of fit test comparing observed data to quantiles of the normal distribution was performed using the Kolmogorov-Smirnov test to determine whether a parametric or non-parametric test would be most appropriate. The Mann-Whitney U test was used to determine significance for data that did not follow a normal distribution. The data are reported as box and whisker plots (mean, median, interquartile range, minimum, and maximum). Data that followed a normal distribution were plotted with bar graphs, presented as mean±SEM and compared using a paired t test. Categorical comparisons were performed using a chi-square test. Correction for the multiplicity of testing was performed by applying Bonferroni's correction when multiple time points/treatment measurements were performed in a sample. Differences between two or more treatment groups were considered significant at $p<0.05$. Survival rates were analyzed with Kaplan-Meier curves. Power analysis was performed to determine the minimum sample size for each experimental group, ($\beta=0.15$; $\alpha=0.05$)

## FIGURE LEGENDS

1. **CSD prevents HF and SCA.** The star indicates p<0.01 vs. HF+ShamCSD. **(A)** *In vivo* picture of guinea pig stellate ganglia (SG) and sympathetic chain running along the right chest wall and anatomical landmarks- rib 1 (R1), rib 2 (R2) and Superior Vena Cava (SVC). The guinea pig SG is located between the first rib and the spine. The SG was accessed from the ventral side via the second intercostal space and is visible as a white fiber running parallel to the spine. **(B)** Representative example of heart rate changes during right [SG(R)] followed by left [SG(L)] stellate ganglionectomy. The box plots summarize the corresponding change in steady-state heart rates. **(C)** Representative immunohistochemistry imaging of excised SG tissue for tyrosine hydroxylase and neurofilament (*red/green*) with DAPI stained nuclei, confirming the presence of sympathetic neurons (scale bar *10 μm*). **(D)** Representative images of gross hearts (top) and corresponding cross-sections (bottom) at 4 weeks. **(E)** Representative M-mode echocardiography. **(F)** Echocardiographic features at 4 weeks (N≥15 per group). Sytolic and diastolic LV internal dimension (LVID) were significantly lower for HF+CSD and HF+mROS-scavenging compared to HF+shamCSD, but the ventricular septal (IVS) and LV posterior wall thickness (LVPW) were not significantly different between groups. Although the relative wall thickness (RWT), end diastolic (EDV) and systolic (ESV) volumes, fractional shortening (FS) and ejection fraction (EF) were significantly lower in both HF+shamCSD and HF+CSD animals, these features were only slightly lower in HF+CSD hearts compared to normal+shamCSD animals, suggesting CSD and mROS scavenging improve these aspects. **(G)** Representative segments from ECG adjudication. Premature ventricular contractions (PVCs), VT and VF were frequently noted in HF+sham, leading to SCA in >70% of the animals (N=68) (**H**). CSD (N=25) and mROS scavenging (N=15) mitigated the incidence of PVCs, VT and SCA (p<0.01; two-tailed log-rank test).

2. **CSD improves autonomic balance and chronotropic competency.** The star indicates p<0.01 vs. HF+ShamCSD. Continuous ECG analysis was performed before (rest), during mild transient β-adrenergic stress with low dose isoproterenol infusion with an automated implanted pump, and 4 hours after stress (recovery). **(A)** Representative heart rate tracings show HF+shamCSD (red) animals had increased heart rate at rest and recovery but reduced heart rate during stress compared to normal+shamCSD (gray), HF+CSD (blue) and HF+mROS-scavenging (green) animals. **(B-D)** The corresponding histograms show that CSD and mROS scavenging lowered the resting heart rate and preserved chronotropic responses (N≥7 animals/group). The box plots summarize the corresponding results for heart rate during rest (**E**) and recovery (**F**), chronotropic response during stress (**G**), heart rate variability, as indexed by SDNN during rest (**H**) and (**I**) recovery, the ratio of the low (LF) and high (HF) frequency bands of the heart rate power spectral density corresponding primarily to sympathetic and parasympathetic tone, respectively, during rest (**J**) and recovery (**K**), and the total power for all frequency bands at rest (**L**) and recovery (**M**) (N>8 per group).

3. **CSD enhances mitochondrial antioxidant capacity and reduces mROS levels in LV myocytes.** The star indicates p<0.01 vs. HF+ShamCSD. **(A)** Representative images over the course of isoproterenol exposure during 1 Hz field stimulation of LV myocytes with GFP-mitoORP1 show progressive increase in GFP signal over time, reflecting increases in ROS level. The lower panel shows co-localization of mitoORP1 and TMRM in the same myocyte, indicating these signals have high specificity for measuring mROS. **(B)** Representative time-lapse tracings of fractional oxidation (Fox) of GFP-mitoORP1 from LV myocytes from normal+shamCSD (grey), HF+shamCSD (red) and HF+CSD (blue) are shown over time at baseline and after (vertical dashed line) exposure to isoproterenol at 1 Hz field stimulation. **(C)** Box plots show baseline mROS levels were highest in the HF+shamCSD myocytes (p<0.001; N>10 myocytes/heart; N>5 hearts/group). **(D)** Increasing endogenous mROS production

using isoproterenol (37°C; 1 Hz) increased mROS in HF+CSD by 10% from baseline whereas, HF+shamCSD myocytes increased by 40% from their already higher baseline values. At the steady state, endogenous ROS levels were significant lower in HF+CSD compared to HF+shamCSD ($p<0.001$). **(E)** The response to an exogenous oxidative stress was tested by exposing myocytes to 1mM tert-butyl hydroperoxide. Scavenging of exogenous ROS was impaired in HF+shamCSD compared to HF+CSD myocytes, indicating CSD improves mitochondrial antioxidant capacity ($p<0.001$). Of note, the HF+CSD group displayed a small by significantly lower ROS scavenging capacity compared to normal+shamCSD ($p<0.01$), consistent with the mildly lower echocardiographic LV function indicating the HF+shamCSD hearts were not similar to normal hearts. **(F)** CSD restored the antioxidant capacity by upregulating the expression of mitochondrial antioxidant enzymes from the thioredoxin and glutathione antioxidant pathways, which were downregulated by pressure overloaded hemodynamic compromise (N>5 hearts/group).

4. **CSD improves LV myocyte function, including enhanced $Ca^{2+}$ handling, sarcomere shortening and β-adrenergic responsiveness.** The star indicates $p<0.01$ vs. HF+ShamCSD. **(A)** Representative $Ca^{2+}$ transients (**A**) from sham+CSD (black), HF+shamCSD (red) and HF+CSD (blue) LV myocytes and derived features of $Ca^{2+}$ transients are shown before **(A-E)** and after **(F-I)** β-adrenergic mediated oxidative stress via exposure to isoproterenol (1 μM; 1 Hz pacing). Compared to normal+shamCSD and HF+CSD, the HF+shamCSD myocytes had higher diastolic $Ca^{2+}$, slower time to 80% of peak upstroke, reduced peak amplitude, and longer time to 80% recovery (T80). The corresponding sarcomere shortening parameters are shown before **(J-N)** and after **(O-R)** stress. Whereas the resting sarcomere length was similar between groups, the HF+shamCSD animals had slower time to 80% of peak upstroke, reduced peak amplitude, and longer T80 ($p<0.01$; N>10 myocytes/heart; N>5 hearts/group). The representative tracings are shown after normalizing resting values.

5. **CSD reduces triggered activity and dispersion of repolarization by reducing ROS-mediated SR $Ca^{2+}$ leak-induced diastolic $Ca^{2+}$ overload.** The star indicates $p<0.01$ vs. HF+ShamCSD. **(A)** In the left panel, the images on top show a snapshot of the GFP signal from a HF+shamCSD myocyte, transduced with GFP-mitoORP1, that exhibited high pacing-induced diastolic $Ca^{2+}$ and dCaTd, followed by DADs and triggered activity within 1 minute of inducing ROS generation by pacing and/or isoproterenol. On right, a representative example is shown for the same experiment in which ROS scavenging with mitoTEMPO reduced diastolic $Ca^{2+}$ and dCaTd and prevented DADs. **(B)** The increase in pacing-induced diastolic $Ca^{2+}$ and dCaTd was increased by ROS and reduced by ROS scavenging, demonstrating a direct relationship. However, despite ROS scavenging, caffeine (which increases RyR open probability) reversibly increased pacing-induced diastolic $Ca^{2+}$ and dCaTd independent of ROS levels. Dantrolene (which stabilizes RyRs during diastole) reduced pacing-induced diastolic $Ca^{2+}$ and dCaTd despite increasing ROS levels. **(C)** The corresponding summary results are shown for mROS levels in HF+shamCSD myocytes at baseline (orange) and before (red) triggered activity. The mROS levels increased by about 30% before the onset of triggered activity. The presence of ROS scavenger (green) abolished high mROS levels, abnormal $Ca^{2+}$ levels, dCaTD and triggered activity in all cells (N>20 myocytes; >5 hearts). Similar experiments could not be performed in normal, HF+CSD and HF+mROS-scavenging myocytes because they had lower mROS levels at baseline and rarely exhibited triggered activity. **(D)** A distribution of diastolic $Ca^{2+}$ levels are shown for all cells during ROS generation and scavenging. Triggered activity was frequently noted when diastolic $Ca^{2+}$ levels exceeded the dashed line. **(E)** Representative example of the correlation between diastolic $Ca^{2+}$ levels and dCaTd in a HF+shamCSD myocyte. The Spearman correlation coefficient is strong (0.77) despite the temporal lag in dCatTd changes with diastolic $Ca^{2+}$ levels. The slope of the linear regression fit is 1.7. **(F)**

Representative example of the weakly positive correlation between peak systolic $Ca^{2+}$ levels and dCaTd in a HF+shamCSD myocyte, likely resulting from impaired mitochondrial calcium loading and consistent with the much better fit of a polynomial compared to a linear function. **(G)** Representative example of the weakly inverse correlation between peak diastolic $Ca^{2+}$ levels and dCaTd in a HF+CSD myocyte. **(H)** The corresponding summary results of the slopes of the linear regression fits and spearman correlation coefficients are shown for HF+shamCSD (red; N>5 hearts; 90 myocytes) and HF+CSD (N>5 hearts; 75 myocytes) animals. **(I)** Representative tracings of the ECG's R to T segment are shown over 24 hours from a Normal+shamCSD, HF+shamCSD, HF+CSD and HF+mROS-scavenging animal. The HF+shamCSD animals exhibit increased dispersion of repolarization compared to HF+CSD and HF+mROS-scavenging animals. **(J)** The corresponding summary results show that the heart rate corrected QT interval (QTc) was not significantly different between HF+shamCSD and HF+CSD at rest and during recovery from stress, but was significantly prolonged compared to Normal+shamCSD ($p<0.01$ vs sham). **(K)** The QT variability index was significantly higher in HF+shamCSD compared to HF+CSD at rest and during recovery from stress (n=>8 animals/group, $p<0.01$). **(L)** The percent PVC over 24 hours was significantly lower in the HF+CSD group compared to HF animals.

6. **Chronic sympathetic stress induced downregulation of mitochondrial antioxidant enzymes leads to mROS-induced SR $Ca^{2+}$ leak from RyRs and diastolic $Ca^{2+}$ overload, which drive SCD and HF pathogenesis; CSD targets these processes to rescue cardioprotection.** Refer to text.

## SUPPLEMENTARY FIGURE LEGENDS

1. **Echocardiographic features over the course of HF development and progression**. Detailed longitudinal echocardiography results from 1-4 weeks showing the progression of structural changes. Section A shows the trends by feature and section B shows the detailed analysis and data points obtained per animal.

2. **CSD has little or no effect in normal animals. (A)** A significant, albeit small decrease in the heart rate was noted in Normal+CSD group compared to Normal+ShamCSD animals, reflecting surgical removal of SG ($p<0.001$). Importantly, no significant difference was observed in **(B)** HRV, **(C)** LF:HF ratio, **(D)** total power **(E)** QTc, and **(F)** QT variability index (QTVI) (ns vs normal).

3. **Frequency distribution of ECG features and corresponding box and whisker plots by groups**. These are shown for pre-stress and post-stress periods.

## REFERENCES


1. DeMazumder D, Tomaselli GF. Molecular and cellular mechanisms of cardiac arrhythmias. In: Hill JA, Olson, E.N., ed. *Muscle 2-volume set: Fundamental biology and mechanisms of disease*. Philadelphia, P.A.: Elsevier Inc.; 2012.
2. Leriche R, Herman L, Fontaine R. Ligature de la coronaire gauche et fonction du coeur après énervation sympathique. *CR Soc Biol*. 1931;107:547
3. Cox W, Lewiston M, Robertson H. The effect of stellate ganglionectomy on the cardiac function of intact dogs: And its effect on the extent of myocardial infarction and on cardiac function following coronary artery occlusion. *Am. Heart J.* 1936;12:285-300
4. Moss AJ, McDonald J. Unilateral cervicothoracic sympathetic ganglionectomy for the treatment of long qt interval syndrome. *N. Engl. J. Med.* 1971;285:903-904
5. Fiorelli A, D'Aponte A, Canonico R, Palladino A, Vicidomini G, Limongelli F, Santini M. T2–t3 sympathectomy versus sympathicotomy for essential palmar hyperhidrosis: Comparison of effects on cardio-respiratory function†. *European Journal of Cardio-Thoracic Surgery*. 2012;42:454-461
6. Ibrahim M, Menna C, Andreetti C, Ciccone AM, D'Andrilli A, Maurizi G, Pomes LM, Cassiano F, Venuta F, Rendina EA. Bilateral single-port sympathectomy: Long-term results and quality of life. *Biomed Res Int*. 2013;2013:348017-348017
7. Schwartz PJ. Cardiac sympathetic denervation to prevent life-threatening arrhythmias. *Nature reviews. Cardiology*. 2014;11:346-353
8. Zanoni FL, Simas R, da Silva RG, Breithaupt-Faloppa AC, Coutinho ESRD, Jatene FB, Moreira LF. Bilateral sympathectomy improves postinfarction left ventricular remodeling and function. *J Thorac Cardiovasc Surg*. 2017;153:855-863
9. Krishnan A, Suarez-Pierre A, Crawford TC, Zhou X, Russell SD, Berger RD, Calkins H, Baumgartner WA, Tandri H, Mandal K. Sympathectomy for stabilization of heart failure due to drug-refractory ventricular tachycardia. *Ann Thorac Surg*. 2018;105:e51-e53
10. Richardson T, Lugo R, Saavedra P, Crossley G, Clair W, Shen S, Estrada JC, Montgomery J, Shoemaker MB, Ellis C, Michaud GF, Lambright E, Kanagasundram AN. Cardiac sympathectomy for the management of ventricular arrhythmias refractory to catheter ablation. *Heart Rhythm*. 2018;15:56-62
11. Zhou M, Liu Y, Xiong L, Quan D, He Y, Tang Y, Huang H, Huang C. Cardiac sympathetic afferent denervation protects against ventricular arrhythmias by modulating cardiac sympathetic nerve activity during acute myocardial infarction. *Med Sci Monit*. 2019;25:1984-1993
12. Aziz H, Nathoo N, Ajlan M, Toscani B, Sirois C, Bracco D, Kornbluth M, Bernier ML. Bilateral cardiac sympathectomy and extrapericardial coil implantation for the management of electrical storm. *JACC. Case reports*. 2021;3:491-495
13. Ardell JL, Foreman RD, Armour JA, Shivkumar K. Cardiac sympathectomy and spinal cord stimulation attenuate reflex-mediated norepinephrine release during ischemia preventing ventricular fibrillation. *JCI Insight*. 2019;4
14. Treatment of ventricular arrhythmia by permanent atrial pacemaker and cardiac sympathectomy. *Ann. Intern. Med.* 1968;68:591-597
15. Vaseghi M, Barwad P, Malavassi Corrales FJ, Tandri H, Mathuria N, Shah R, Sorg JM, Gima J, Mandal K, Sàenz Morales LC, Lokhandwala Y, Shivkumar K. Cardiac sympathetic denervation for refractory ventricular arrhythmias. *J Am Coll Cardiol*. 2017;69:3070-3080

16. Meng L, Shivkumar K, Ajijola O. Autonomic regulation and ventricular arrhythmias. *Current treatment options in cardiovascular medicine*. 2018;20:38

17. Boukens BJD, Dacey M, Meijborg VMF, Janse MJ, Hadaya J, Hanna P, Swid MA, Opthof T, Ardell JL, Shivkumar K, Coronel R. Mechanism of ventricular premature beats elicited by left stellate ganglion stimulation during acute ischaemia of the anterior left ventricle. *Cardiovascular research*. 2021;117:2083-2091

18. Butrous GS, Gough WB, Restivo M, Yang H, el-Sherif N. Adrenergic effects on reentrant ventricular rhythms in subacute myocardial infarction. *Circulation*. 1992;86:247-254

19. Tygesen H, Wettervik C, Claes G, Drott C, Emanuelsson H, Solem J, Lomsky M, Radberg G, Wennerblom B. Long-term effect of endoscopic transthoracic sympathicotomy on heart rate variability and qt dispersion in severe angina pectoris. *Int J Cardiol*. 1999;70:283-292

20. Yalin K, Liosis S, Palade E, Fink T, Schierholz S, Sawan N, Eitel C, Heeger CH, Sciacca V, Sano M, Vogler J, Tilz RR. Cardiac sympathetic denervation in patients with nonischemic cardiomyopathy and refractory ventricular arrhythmias: A single-center experience. *Clinical Research in Cardiology*. 2020

21. Dey S, DeMazumder D, Sidor A, Foster DB, O'Rourke B. Mitochondrial ros drive sudden cardiac death and chronic proteome remodeling in heart failure. *Circ Res*. 2018;123:356-371

22. Stengl M. Experimental models of spontaneous ventricular arrhythmias and of sudden cardiac death. *Physiol. Res.* 2010;59 Suppl 1:S25-31

23. Lloyd-Jones DM, Larson MG, Leip EP, Beiser A, D'Agostino RB, Kannel WB, Murabito JM, Vasan RS, Benjamin EJ, Levy D, Framingham Heart S. Lifetime risk for developing congestive heart failure: The framingham heart study. *Circulation*. 2002;106:3068-3072

24. Dey S, Sidor A, O'Rourke B. Compartment-specific control of reactive oxygen species scavenging by antioxidant pathway enzymes. *The Journal of biological chemistry*. 2016;291:11185-11197

25. Frolkis JP, Pothier CE, Blackstone EH, Lauer MS. Frequent ventricular ectopy after exercise as a predictor of death. *New England Journal of Medicine*. 2003;348:781-790

26. Kourie JI. Interaction of reactive oxygen species with ion transport mechanisms. *The American journal of physiology*. 1998;275:C1-24

27. Zima AV, Blatter LA. Redox regulation of cardiac calcium channels and transporters. *Cardiovasc Res*. 2006;71:310-321

28. Terentyev D, Gyorke I, Belevych AE, Terentyeva R, Sridhar A, Nishijima Y, de Blanco EC, Khanna S, Sen CK, Cardounel AJ, Carnes CA, Gyorke S. Redox modification of ryanodine receptors contributes to sarcoplasmic reticulum $ca^{2+}$ leak in chronic heart failure. *Circulation research*. 2008;103:1466-1472

29. Liu T, Yang N, Sidor A, O'Rourke B. Mcu overexpression rescues inotropy and reverses heart failure by reducing sr $ca(^{2+})$ leak. *Circ. Res.* 2021;128:1191-1204

30. Yan Y, Liu J, Wei C, Li K, Xie W, Wang Y, Cheng H. Bidirectional regulation of $ca^{2+}$ sparks by mitochondria-derived reactive oxygen species in cardiac myocytes. *Cardiovasc Res*. 2008;77:432-441

31. Ho HT, Stevens SC, Terentyeva R, Carnes CA, Terentyev D, Gyorke S. Arrhythmogenic adverse effects of cardiac glycosides are mediated by redox modification of ryanodine receptors. *The Journal of physiology*. 2011;589:4697-4708

32. DeMazumder D, Limpitikul WB, Dorante M, Dey S, Mukhopadhyay B, Zhang Y, Moorman JR, Cheng A, Berger RD, Guallar E, Jones SR, Tomaselli GF. Entropy of cardiac repolarization predicts

ventricular arrhythmias and mortality in patients receiving an implantable cardioverter-defibrillator for primary prevention of sudden death. *Europace*. 2016;18:1818-1828

33. Liu H, Zhao Y, Xie A, Kim TY, Terentyeva R, Liu M, Shi G, Feng F, Choi BR, Terentyev D, Hamilton S, Dudley SC, Jr. Interleukin-1β, oxidative stress, and abnormal calcium handling mediate diabetic arrhythmic risk. *JACC Basic Transl Sci*. 2021;6:42-52

34. Xie A, Zhou A, Liu H, Shi G, Liu M, Boheler KR, Dudley SC, Jr. Mitochondrial $ca^{2+}$ flux modulates spontaneous electrical activity in ventricular cardiomyocytes. *PLoS One*. 2018;13:e0200448

35. Xie A, Song Z, Liu H, Zhou A, Shi G, Wang Q, Gu L, Liu M, Xie LH, Qu Z, Dudley SC, Jr. Mitochondrial $ca(^{2+})$ influx contributes to arrhythmic risk in nonischemic cardiomyopathy. *J Am Heart Assoc*. 2018;7

36. Song LS, Wang SQ, Xiao RP, Spurgeon H, Lakatta EG, Cheng H. Beta-adrenergic stimulation synchronizes intracellular $ca(^{2+})$ release during excitation-contraction coupling in cardiac myocytes. *Circulation research*. 2001;88:794-801

37. Venetucci LA, Trafford AW, Eisner DA. Increasing ryanodine receptor open probability alone does not produce arrhythmogenic calcium waves: Threshold sarcoplasmic reticulum calcium content is required. *Circulation research*. 2007;100:105-111

38. Zorov DB, Juhaszova M, Sollott SJ. Mitochondrial reactive oxygen species (ros) and ros-induced ros release. *Physiol Rev*. 2014;94:909-950

39. Curran J, Tang L, Roof SR, Velmurugan S, Millard A, Shonts S, Wang H, Santiago D, Ahmad U, Perryman M, Bers DM, Mohler PJ, Ziolo MT, Shannon TR. Nitric oxide-dependent activation of camkii increases diastolic sarcoplasmic reticulum calcium release in cardiac myocytes in response to adrenergic stimulation. *PloS one*. 2014;9:e87495

40. Curran J, Hinton MJ, Rios E, Bers DM, Shannon TR. Beta-adrenergic enhancement of sarcoplasmic reticulum calcium leak in cardiac myocytes is mediated by calcium/calmodulin-dependent protein kinase. *Circulation research*. 2007;100:391-398

41. Schlotthauer K, Bers DM. Sarcoplasmic reticulum $ca(^{2+})$ release causes myocyte depolarization. Underlying mechanism and threshold for triggered action potentials. *Circulation research*. 2000;87:774-780

42. Liu M, Liu H, Dudley SC, Jr. Reactive oxygen species originating from mitochondria regulate the cardiac sodium channel. *Circ Res*. 2010;107:967-974

43. Liu M, Sanyal S, Gao G, Gurung IS, Zhu X, Gaconnet G, Kerchner LJ, Shang LL, Huang CL, Grace A, London B, Dudley SC, Jr. Cardiac na+ current regulation by pyridine nucleotides. *Circ Res*. 2009;105:737-745

44. Droge W. Free radicals in the physiological control of cell function. *Physiological reviews*. 2002;82:47-95

45. Hool LC. Evidence for the regulation of l-type $ca^{2+}$ channels in the heart by reactive oxygen species: Mechanism for mediating pathology. *Clinical and experimental pharmacology & physiology*. 2008;35:229-234

46. Brand MD, Affourtit C, Esteves TC, Green K, Lambert AJ, Miwa S, Pakay JL, Parker N. Mitochondrial superoxide: Production, biological effects, and activation of uncoupling proteins. *Free radical biology & medicine*. 2004;37:755-767

47. Wei AC, Aon MA, O'Rourke B, Winslow RL, Cortassa S. Mitochondrial energetics, ph regulation, and ion dynamics: A computational-experimental approach. *Biophysical journal*. 2011;100:2894-2903

48. Song M, Chen Y, Gong G, Murphy E, Rabinovitch PS, Dorn GW, 2nd. Super-suppression of mitochondrial reactive oxygen species signaling impairs compensatory autophagy in primary mitophagic cardiomyopathy. *Circ. Res.* 2014;115:348-353

49. Gehi A, Haas D, Fuster V. Primary prophylaxis with the implantable cardioverter-defibrillator: The need for improved risk stratification. *JAMA.* 2005;294:958-960

50. Bardy GH, Lee KL, Mark DB, Poole JE, Packer DL, Boineau R, Domanski M, Troutman C, Anderson J, Johnson G, McNulty SE, Clapp-Channing N, Davidson-Ray LD, Fraulo ES, Fishbein DP, Luceri RM, Ip JH. Amiodarone or an implantable cardioverter-defibrillator for congestive heart failure. *N. Engl. J. Med.* 2005;352:225-237

Figure 1

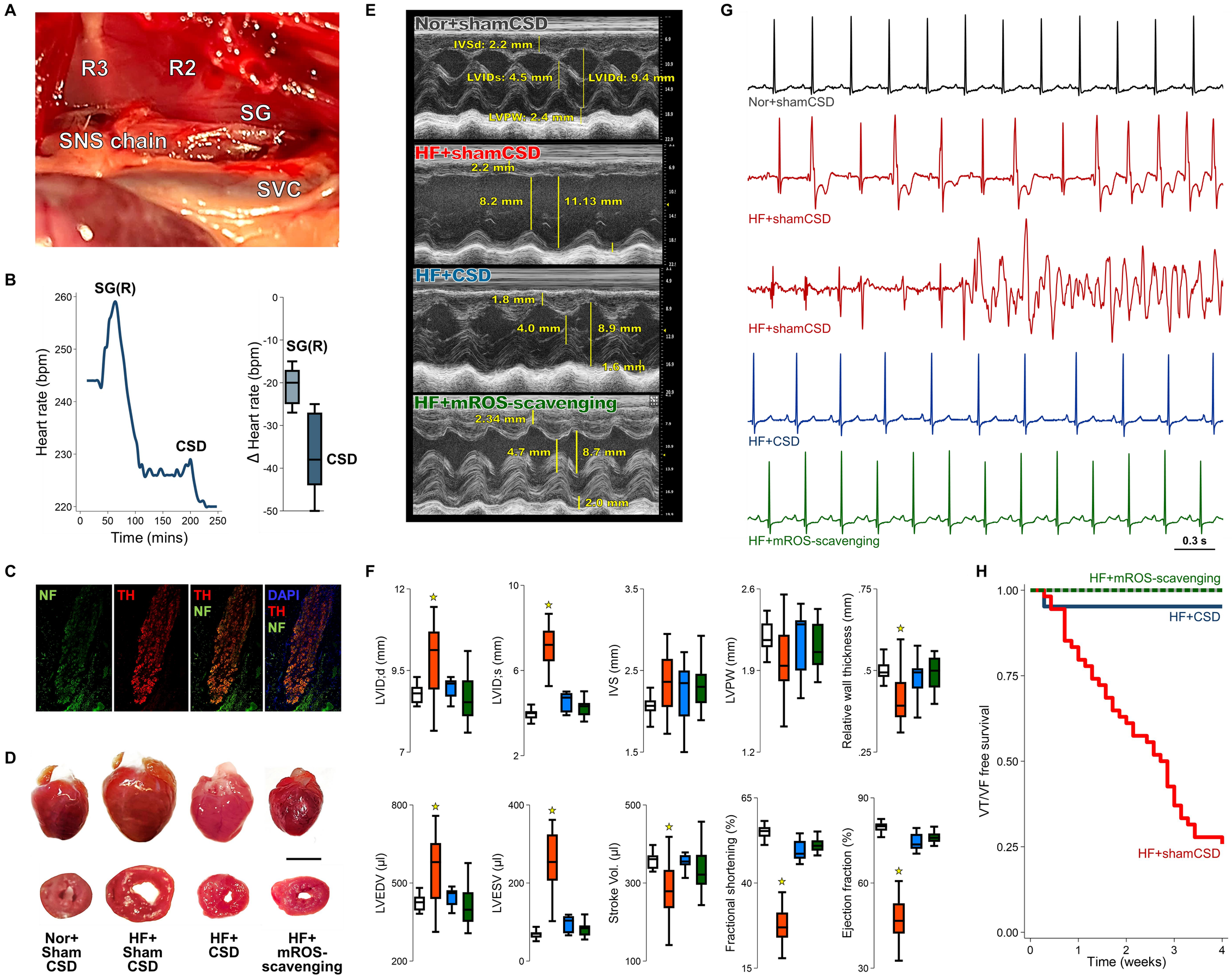
A
R3
R2
SG
SNS chain
SVC
B
SG(R)
CSD
Heart rate (bpm)
Time (mins)
Δ Heart rate (bpm)
SG(R)
CSD
E
Nor+shamCSD
IVSd: 2.2 mm
LVIDs: 4.5 mm
LVIDd: 9.4 mm
LVPW: 2.4 mm
HF+shamCSD
2.2 mm
8.2 mm
11.13 mm
HF+CSD
1.8 mm
4.0 mm
8.9 mm
1.6 mm
HF+mROS-scavenging
2.34 mm
4.7 mm
8.7 mm
2.0 mm
G
Nor+shamCSD
HF+shamCSD
HF+shamCSD
HF+CSD
HF+mROS-scavenging
0.3 s
C
NF
TH
TH
NF
DAPI
TH
NF
D
Nor+ Sham CSD
HF+ Sham CSD
HF+ CSD
HF+ mROS-scavenging
F
LVID;d (mm)
LVID;s (mm)
IVS (mm)
LVPW (mm)
Relative wall thickness (mm)
LVEDV (µl)
LVESV (µl)
Stroke Vol. (µl)
Fractional shortening (%)
Ejection fraction (%)
H
HF+mROS-scavenging
HF+CSD
HF+shamCSD
VT/VF free survival
Time (weeks)

**Figure 2**

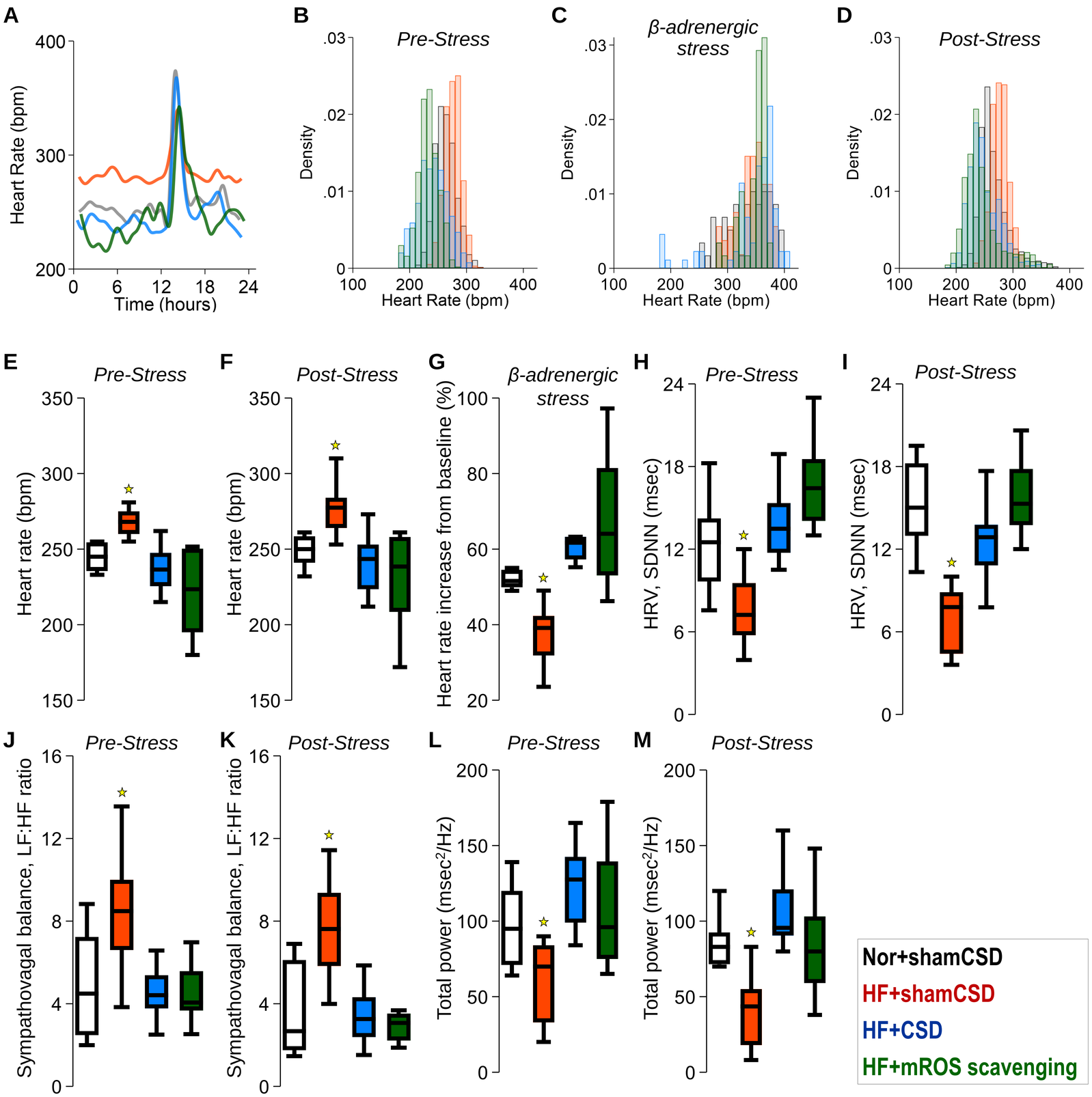
A
Heart Rate (bpm)
Time (hours)
B
Pre-Stress
Density
Heart Rate (bpm)
C
β-adrenergic stress
Density
Heart Rate (bpm)
D
Post-Stress
Density
Heart Rate (bpm)
E
Pre-Stress
Heart rate (bpm)
F
Post-Stress
Heart rate (bpm)
G
β-adrenergic stress
Heart rate increase from baseline (%)
H
Pre-Stress
HRV, SDNN (msec)
I
Post-Stress
HRV, SDNN (msec)
J
Pre-Stress
Sympathovagal balance, LF:HF ratio
K
Post-Stress
Sympathovagal balance, LF:HF ratio
L
Pre-Stress
Total power (msec²/Hz)
M
Post-Stress
Total power (msec²/Hz)
Nor+shamCSD
HF+shamCSD
HF+CSD
HF+mROS scavenging

Figure 3

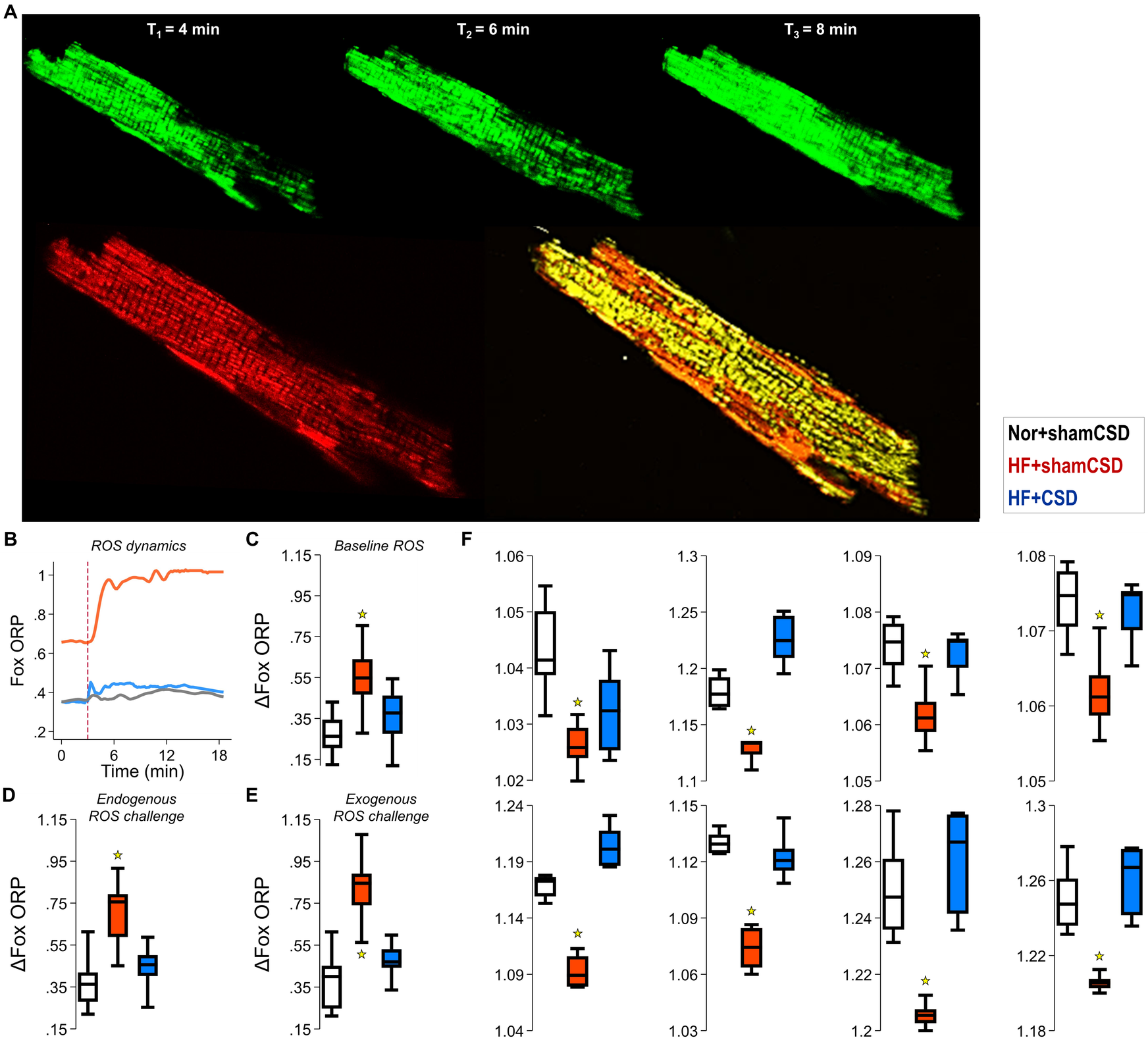
A
$T_1$ = 4 min
$T_2$ = 6 min
$T_3$ = 8 min
Nor+shamCSD
HF+shamCSD
HF+CSD
B
ROS dynamics
Fox ORP
Time (min)
C
Baseline ROS
ΔFox ORP
D
Endogenous ROS challenge
ΔFox ORP
E
Exogenous ROS challenge
ΔFox ORP
F

**Figure 4**

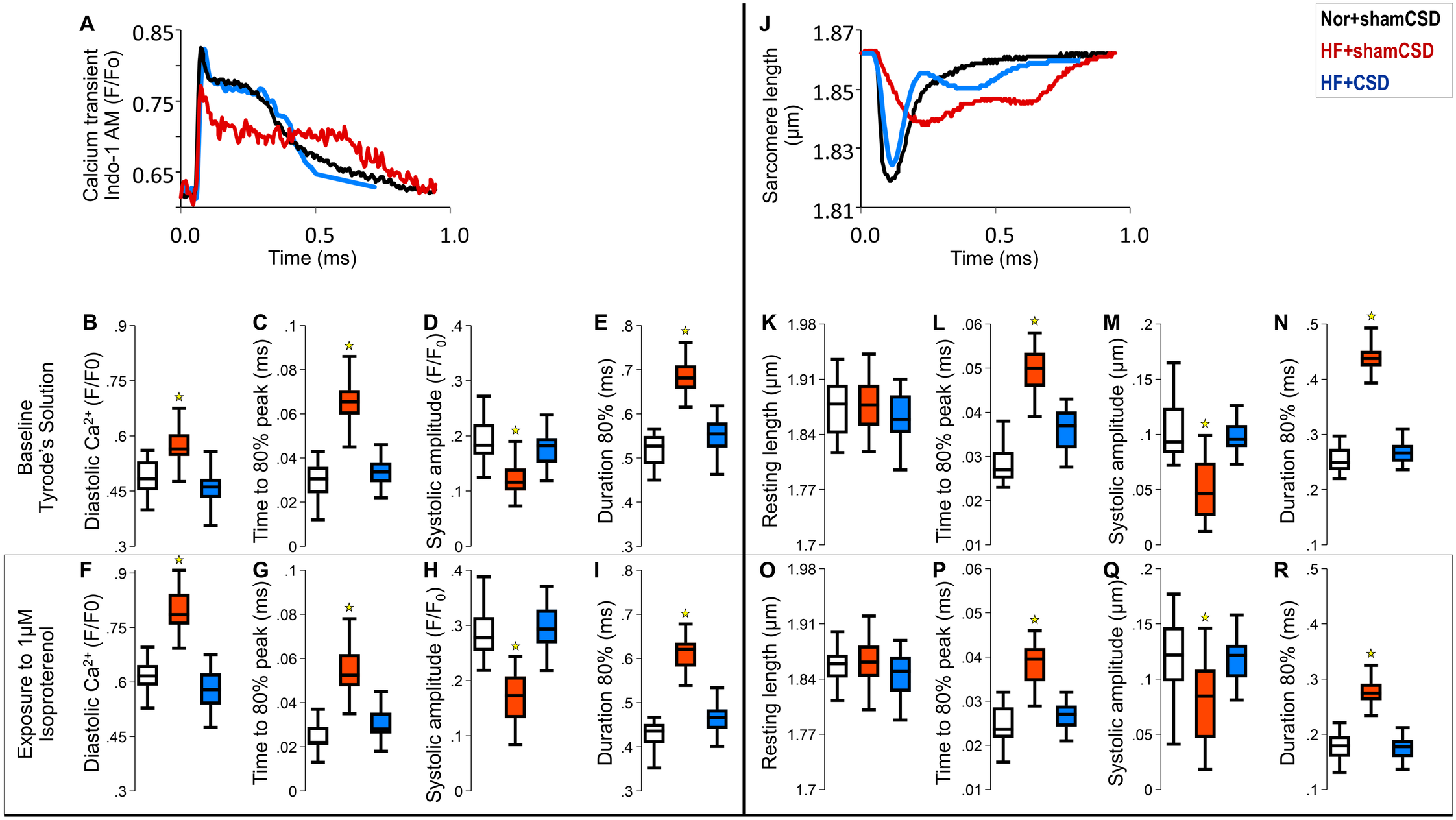
A
Calcium transient Indo-1 AM (F/Fo)
0.85
0.75
0.65
0.0
0.5
1.0
Time (ms)
J
Sarcomere length (µm)
1.87
1.85
1.83
1.81
0.0
0.5
1.0
Time (ms)
Nor+shamCSD
HF+shamCSD
HF+CSD
Baseline Tyrode's Solution
Exposure to 1µM Isoproterenol
B
Diastolic Ca2+ (F/F0)
C
Time to 80% peak (ms)
D
Systolic amplitude (F/F0)
E
Duration 80% (ms)
F
Diastolic Ca2+ (F/F0)
G
Time to 80% peak (ms)
H
Systolic amplitude (F/F0)
I
Duration 80% (ms)
K
Resting length (µm)
L
Time to 80% peak (ms)
M
Systolic amplitude (µm)
N
Duration 80% (ms)
O
Resting length (µm)
P
Time to 80% peak (ms)
Q
Systolic amplitude (µm)
R
Duration 80% (ms)

Figure 5

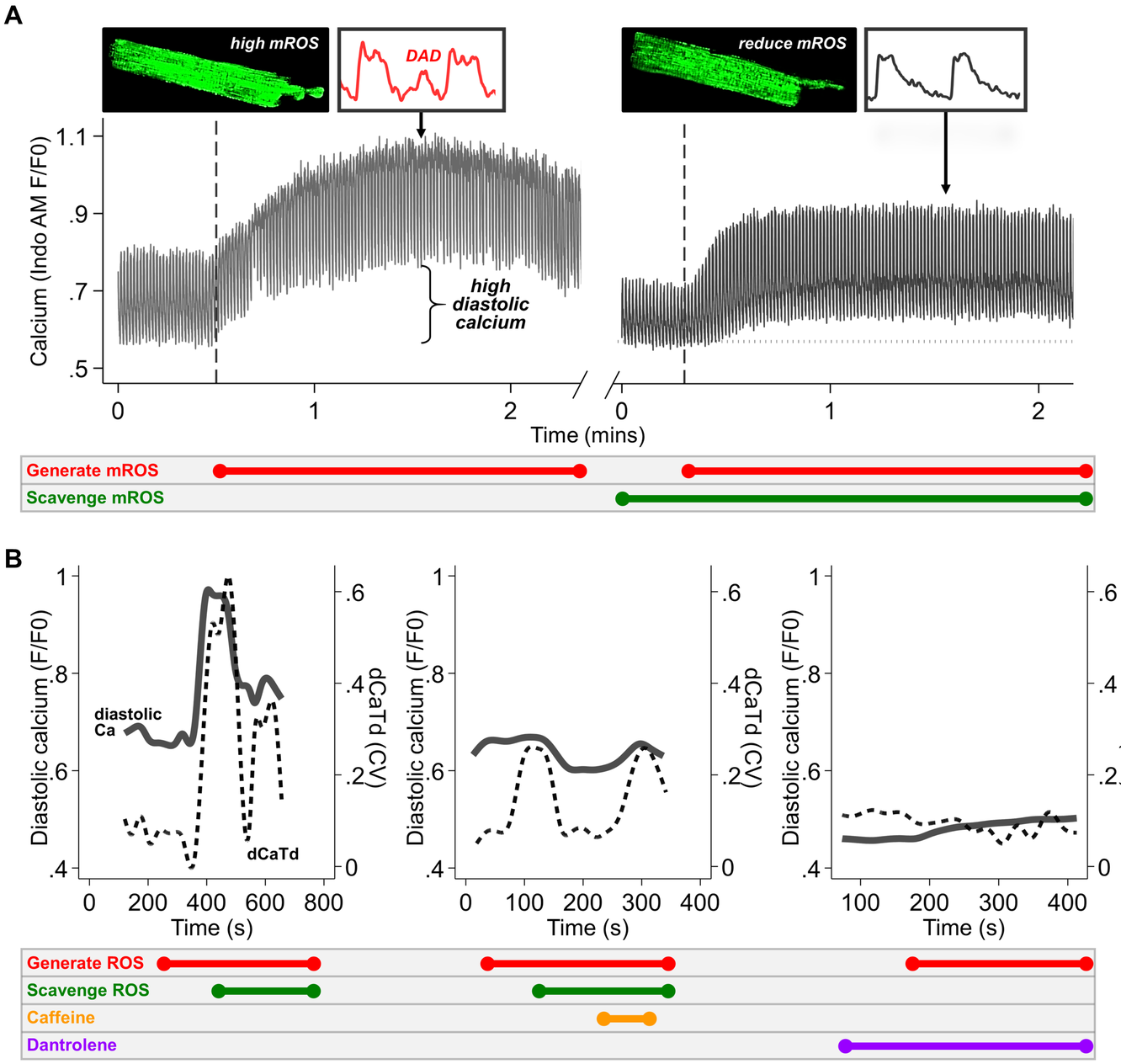
A
high mROS
DAD
reduce mROS
Calcium (Indo AM F/F0)
high diastolic calcium
Time (mins)
Generate mROS
Scavenge mROS
B
Diastolic calcium (F/F0)
dCaTd (CV)
diastolic Ca
dCaTd
Time (s)
Generate ROS
Scavenge ROS
Caffeine
Dantrolene

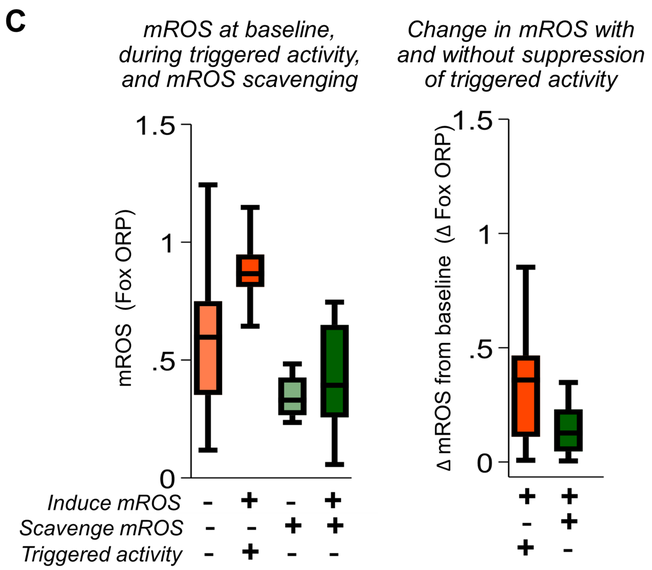
C
mROS at baseline, during triggered activity, and mROS scavenging
Change in mROS with and without suppression of triggered activity
mROS (Fox ORP)
Δ mROS from baseline (Δ Fox ORP)
Induce mROS
Scavenge mROS
Triggered activity

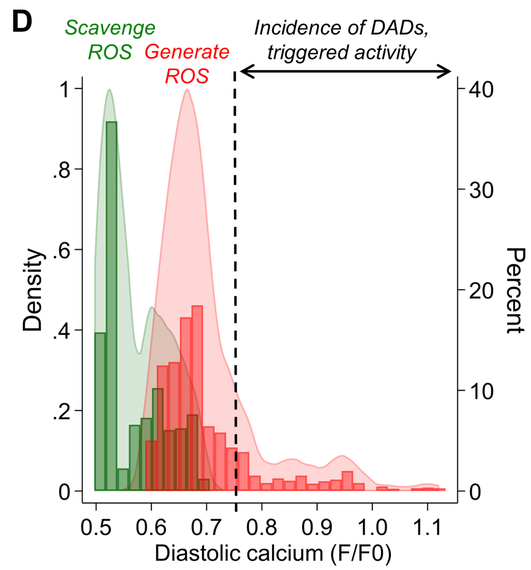
D
Scavenge ROS
Generate ROS
Incidence of DADs, triggered activity
Density
Percent
Diastolic calcium (F/F0)

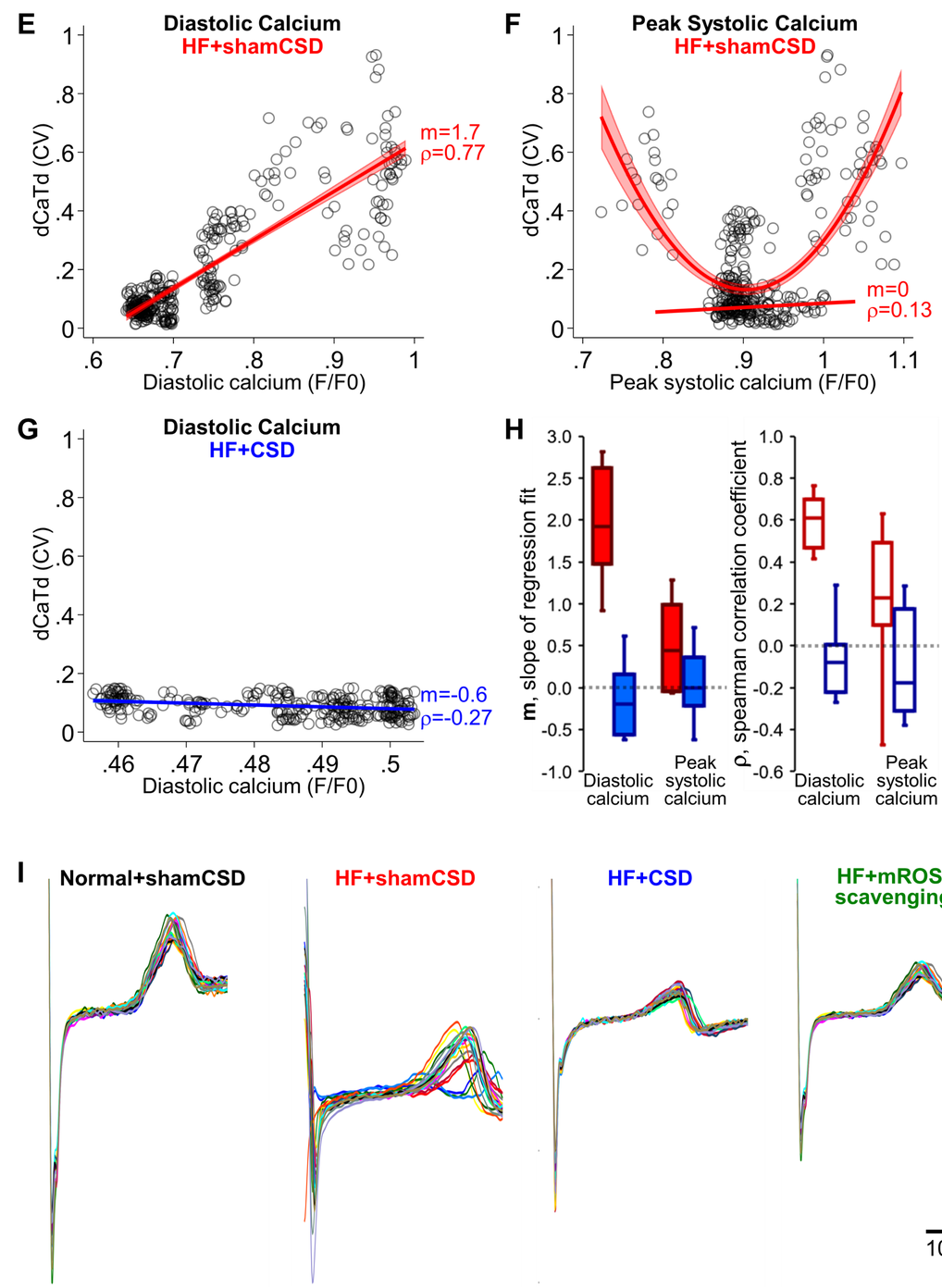
E
Diastolic Calcium
HF+shamCSD
m=1.7
ρ=0.77
dCaTd (CV)
Diastolic calcium (F/F0)
F
Peak Systolic Calcium
HF+shamCSD
m=0
ρ=0.13
Peak systolic calcium (F/F0)
G
Diastolic Calcium
HF+CSD
m=-0.6
ρ=-0.27
H
m, slope of regression fit
ρ, spearman correlation coefficient
Diastolic calcium
Peak systolic calcium


I
Normal+shamCSD
HF+shamCSD
HF+CSD
HF+mROS-scavenging
100 ms

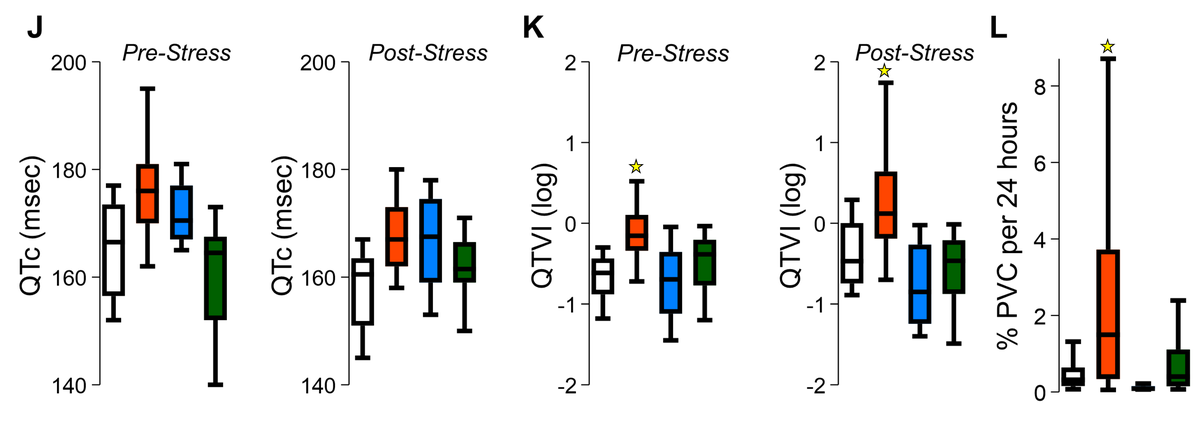
J
Pre-Stress
Post-Stress
QTc (msec)
K
QTVI (log)
L
% PVC per 24 hours

**Figure 6**

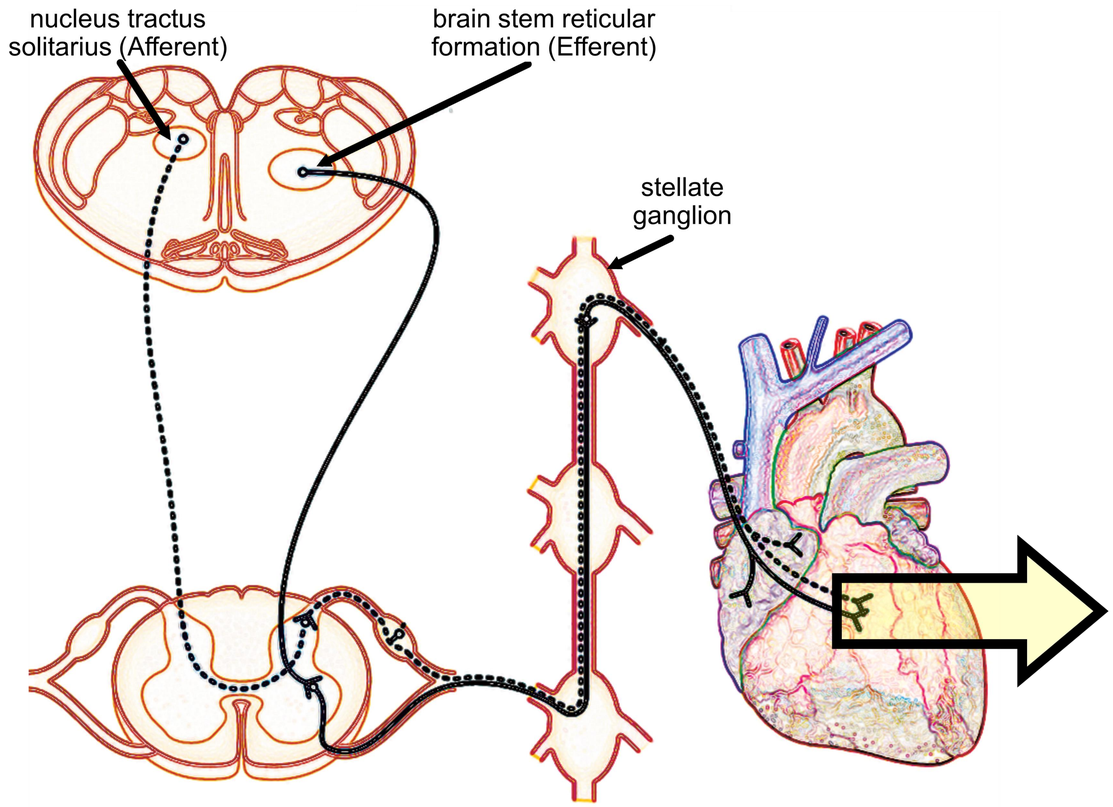


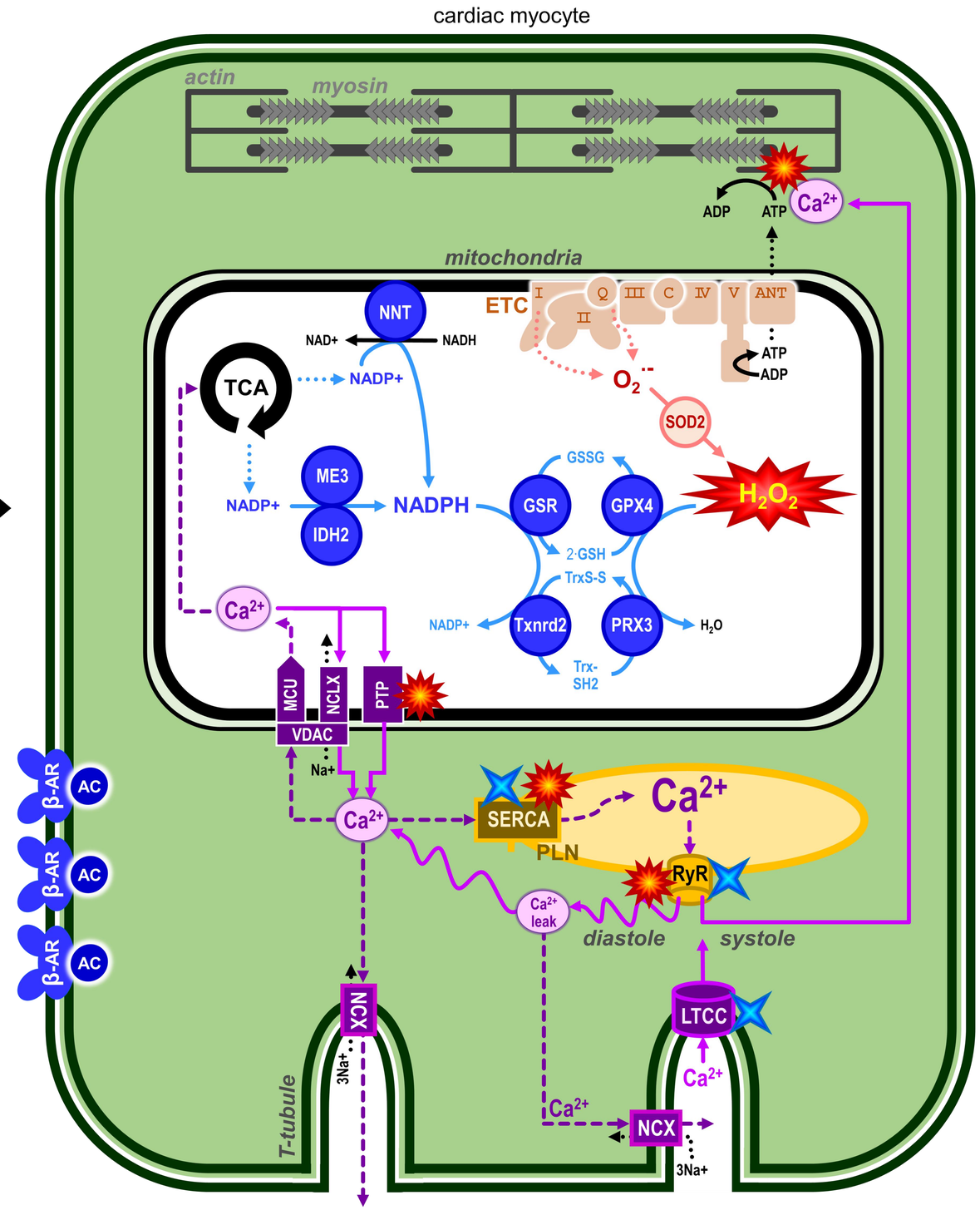


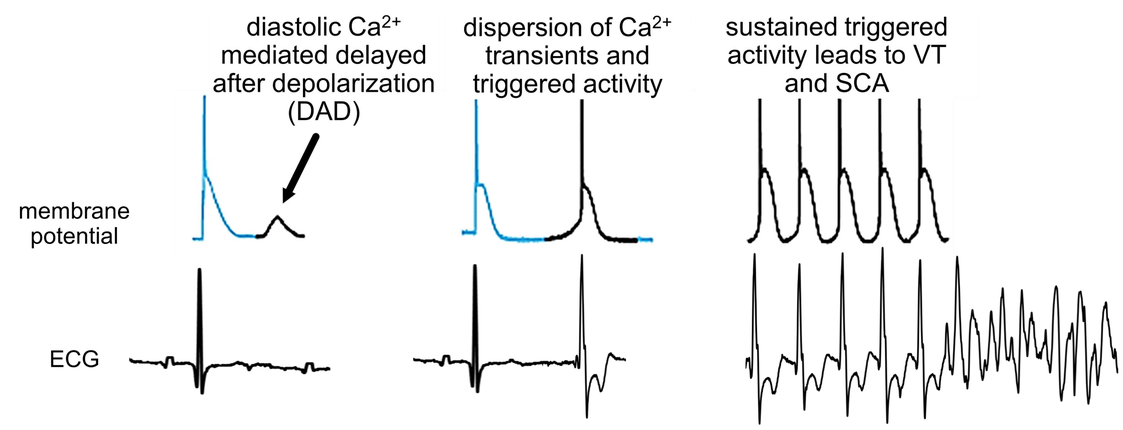


## Legend

| | |
|---|---|
| | Mitochondrial antioxidant enzymes are downregulated by chronic sympathetic β-adrenergic receptor (β-AR) mediated stress but upregulated by CSD to prevent HF and SCA (refer to text). |
| | Key calcium handling proteins modified by ROS. |
| | Key targets of β-AR adenylate cyclase (AC)-cAMP-protein kinase A (PKA) signaling pathway |
| **TCA** | The citric acid cycle. |
| **ETC** | Electron transport chain. |
| **SERCA** | Sarcoplasmic reticulum (SR) $Ca^{2+}$-ATPase transports calcium from the cytosol into the SR. |
| **PLN** | Phospholamban (unphosphorylated) inhibits SERCA when unphosphorylated, but when phosphorylated by β-AR-AC-cAMP-PKA signaling, it does not inhibit SERCA and as such, increases SERCA activity, which lowers diastolic $Ca^{2+}$ and increases SR $Ca^{2+}$ load. |
| **RyR** | The ryanodine receptor (type 2), an ion channel, is opened by membrane depolarization during systole to allow SR $Ca^{2+}$ to enter the cytosol and bind to troponin, which shifts tropomyosin and allows the myosin ATPase to bind to actin, enabling cardiac excitation-contraction coupling. |
| **LTCC** | L-type $Ca^{2+}$ channel allows extracellular $Ca^{2+}$ to enter the cells and induce $Ca^{2+}$ induced SR $Ca^{2+}$ release via the RyRs. |
| **NCX** | Sodium-$Ca^{2+}$ exchanger rapidly transports a cytosolic $Ca^{2+}$ ion to the extracellular space in exchange for 3 sodium ions, generating an inward current during high intracellular $Ca^{2+}$ levels. |
| **MCU** | Mitochondrial $Ca^{2+}$ uniporter in the inner membrane allows $Ca^{2+}$ to enter the mitochondria. |
| **NCLX** | Mitochondrial sodium-$Ca^{2+}$ exchanger, located in the inner membrane, is the major pathway for $Ca^{2+}$ efflux from the mitochondrial matrix and the primary regulator of mitochondrial $Ca^{2+}$, which in turn, regulates the rate of ATP production via the TCA and ETC. |
| **PTP** | Mitochondrial permeability transition pore in the inner membrane allows $Ca^{2+}$ efflux to cytosol. |
| **VDAC** | Mitochondrial voltage-dependent anion-selective channel in the outer membrane is a general diffusion pore for small hydrophilic molecules including $Ca^{2+}$. |